A Parallel Method for Anatomical Structure Segmentation based on 3D Seeded Region Growing

Paulo Lacerda*, José Gonzalez*, Nazareth Rocha†, Flavio Seixas*, Célio Albuquerque*, Esteban Clua*, Aura Conci*
*Computing Institute, Federal Fluminense University, RJ, Brazil
† Biomedical Institute, Federal Fluminense University, RJ, Brazil
{*placerda, jgonzalez, nrocha, fseixas, celioalbuquerque, esteban, aconci*}*@id.uff.br*

***Abstract*—Medical images are important elements for the diagnosis of diseases. Computer Aided Diagnostic has evolved in recent years along with the processing capacity of computers as well as the emergence of new computational techniques. Segmentation is a valuable approach for identifying a specific area in human body images, such as the lungs and heart. This work proposes an algorithm to segment anatomical structures using parallel 3D region growing. Experiments using different Computer Tomography scans show that the proposed approach can run 150 times faster than the typical sequential region growing algorithm while providing good results in the identification of the target region.**

***Index Terms*—segmentation, Compute Unified Device Architecture (CUDA), region growing, Computer Aided Diagnosis (CAD), Digital Imaging Communications in Medicine (DICOM).**

I. Introduction

Technological evolution has brought several benefits to medicine and health studies. Improvements in systems, devices and the quality of imaging examinations increase digital information. This large amount of data contributes to more accurate studies and diagnoses, as in [1]. In this sense, precise anatomical localization is crucial for diagnosis as well as for therapy planning.

Computed Tomography (CT) examinations present slices of the analyzed object, producing detailed anatomical information allowing to discriminate pathological from healthy tissue [2]. This provides greater quality and quantity of data and permits the recognition of structures that would be difficult to perceive in other methods of examination.

In computed tomography, an X-ray beam is emitted from different angles around the area of interest, and an image (or slice) is reconstructed with data processing, showing a cross-section of tissues and organs. The image can be stored in DICOM format [3], where pixels are represented in terms of the mean attenuation of the tissue, in Hounsfield units (HU). Water has an attenuation of 0 HU, while air have -1000 HU, bone have typically +400 HU or greater, and metallic implants are usually +1000 HU [4].

According with Hounsfield [5], CT has some advantages over conventional X-rays images in the localization of anatomical structures. While X-ray superimpose the absorption values of many tissues along a ray, CT records X-ray attenuation for small volumetric elements independently, providing accurate localization of objects in depth.

Thus, CT images allow radiologists and other physicians to identify internal structures and see their shape, size, density and texture. However, some features of CT images that may be of great relevance are not perceived by the human eye, making it necessary to use some specific tools for identification. In this sense, computational methods of image processing and artificial intelligence have been used to create more complex methodologies to help in the diagnosis. These methodologies are known as Computer Aided Diagnosis (CADs) methods. Accordingly [6] "diagnosis based on chest CT images, assisted by computer has been a remarkable and revolutionary step in the early detection of pulmonary abnormalities". Works presented in [7] [8] [9] show surveys about the last recent applications of CADs methods using CT images to detect lung diseases.

In this work, we propose a new segmentation method capable of quickly and efficiently identifying the anatomical structure in computed tomography images, by growing the region in parallel and three dimensions using a 26-neighborhood window. Achieving a performance gain of more than 150 times that of the sequential algorithm. This method allows the automatic extraction of information about the target region. The evaluation of the proposed method is carried out based on its performance in segment chest CT images of rodents.

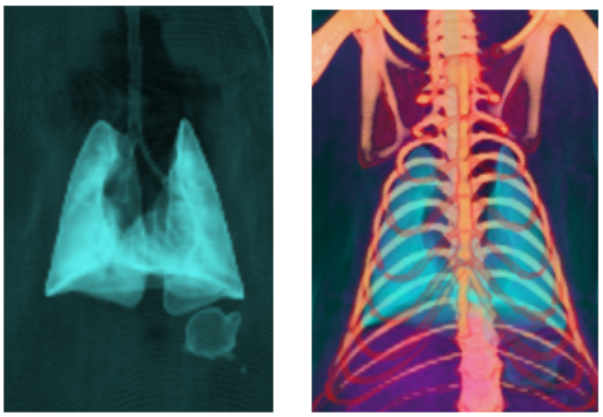

Fig. 1. 3D reconstruction of airways, and airways and bones of a rodent.

This work is supported in part by CNPq, INCT-MACC, CAPES, FAPERJ and CGI/FAPESP.

978-1-7281-6926-2/20/$31.00 ©2020 IEEE

Fig. 1 shows an example of a three-dimensional reconstruction of the airways regions of one of the rodents used in the evaluation of the proposed method. The image was created using the three-dimensional reconstruction function of RadiAnt DICOM Viewer software [10].

Lung segmentation can be very useful in the diagnosis of diseases such as emphysema and pneumonia. The lung areas can be divided into four types: hypo-aerated, hyper-aerated, norm-aerated and non-aerated, according to the density of the material contained in this area. The volume of these areas can be related to the occurrence of lung diseases, such as pulmonary emphysema and pneumonia. Figure 2 shows the respective initial and final HU values of the ranges to hypo-aerated, hyper-aerated, norm-aerated and non-aerated intervals.

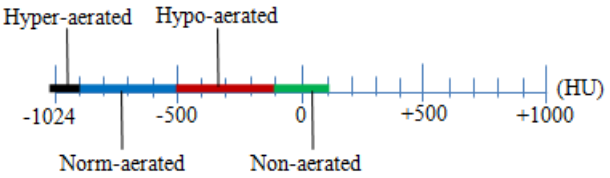

Fig. 2. Hypo-aerated, hyper-aerated, norm-aerated and non-aerated values.

This paper is organized as follows: related works are presented in Section 2; the proposed region growing method in Section 3; the results are presented in detail in Section 4; and finally, the conclusions in Section 5.

II. Related Works

A study of different techniques of image segmentation on chest CT images is presented in [6]. The selected method for this was a region growing algorithm. The authors concludes that the algorithm can be used in CAD system to help radiologist in early diagnosing of lung diseases, and can also be used to early diagnose of other benign or malignant pathologies from other organs, such as liver, brain or spine. Some indications about the selection of seed pixel was made as well in [6].

In [11] chest CT imaging exams of lung were used to extract resources for the classification of lung diseases, such as the classification of pneumonia, emphysema, and bronchitis. Algorithms of supervised machine learning and image filters were also used.

A fully automatic method for identifying the lungs in three-dimensional (3-D) pulmonary X-ray CT images was presented in [12]. The method has three main steps. First, the lung region is extracted from the CT images by gray-level thresholds. Then, the left and right lungs are separated by identifying the anterior and posterior junctions by dynamic programming. Finally, a sequence of morphological operations are used to smooth the irregular boundary along the mediastinum in order to achieve results consistent with those obtained by manual analysis, in which only the most central pulmonary arteries are excluded from the lung region.

In [13] it is presented an extensive survey about CAD system to detect multiples diseases in the chest X-rays. It reviews the datasets of chest X-rays, image segmentation techniques, and artificial intelligence that were used in others works.

III. Methodology

Image segmentation is the process of separating an image in parts for a more meaningful representation. This can be used either to search objects or regions within the image, or to determine the borders of those regions. Thus, regions are grouped or divided depending on whether or not their pixels have similar characteristics in terms of some significant properties for the analysis to be made, such as color, objects form and texture. [14].

Adjacent regions are significantly different with respect to the same characteristic [15]. There are several automatic or semi-automatic algorithms for this purpose. The majority of them are based on few basics strategies and combinations, as multi-thresholding, region growing, edge detection, fusion and division, morphological image reconstruction, clustering and dual clustering, partial differential equation-based methods, graph partitioning methods and compression-based methods. Image segmentation task in this work is based on region growing method [16].

A. 3D Seeded Region Growing

Image segmentation based on region growing are best suited for grouping sets of voxels that meet a given criterion of homogeneity. The region growing method will add new voxels iteratively around the seed element in case they have similar characteristics. Consequently, the border points of the region will exhibit features possibly less similar to the seed voxel as it moves away from it. The homogeneity criterion establishes the type of features that will be used to evaluate the similarity or dissimilarity between the seed point and the current point in analysis [17].

In the seeded region growing method [16] the scanned object slices are loaded into memory along with manually selected seeds coordinates. These seeds make up the first voxels that represents the region to be segmented and a feature vector is calculated for each seed.

After loading the seeds and calculating their feature vectors, the region growing loop begins. At each iteration of the loop, each voxel that is neighbor to the region has its feature vector calculated and, if the euclidean distance between its vector and the seed's feature is less than a predefined threshold value, it is added to the region. These steps are repeated until no more voxels are added to the region. Fig. 3 flowchart shows an overview of this method.

The method performs volumetric growth, that is, the region growing algorithm not only considers the pixels in the same 2D section to make the growth, but also the voxels that are in the neighborhood in three dimensions. In the proposed method, the neighborhood, also called connectivity, is a 26-neighborhood. Besides the voxels on the left/right, top/bottom, front/back of the current voxel in a 6-neighborhood, it also considers the voxels on the two diagonals from the current

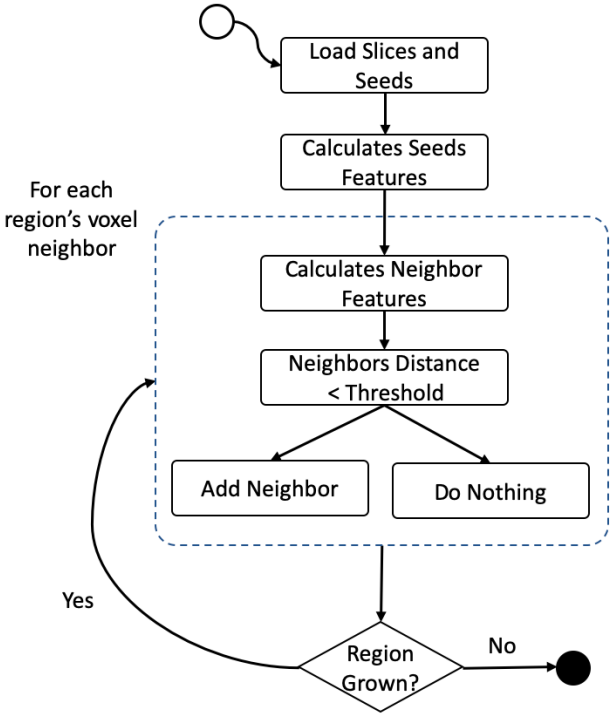

Fig. 3. Region Growing Method Flowchart.

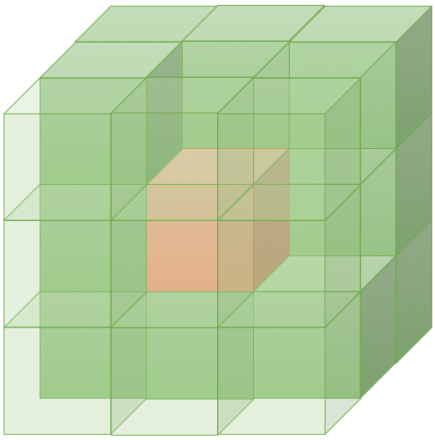

Fig. 4. 26-connected neighborhood of a voxel.

voxel. Fig. 4 illustrates what would be a 26-neighborhood (green voxels), of the voxels being analyzed (orange voxels).

In the beginning, only the HU voxel intensity value was considered as a feature for the segmentation, but the results obtained were not adequate, since the segmented region was either significantly smaller than manual segmentation, or it overflowed outside the region of interest, as shown in the red area in Fig. 5.

To improve segmentation, other features were included. Each feature vector is made up of five elements, where the first feature represents the voxel's HU value. CT slices are grayscale images, where each pixel value has a single value

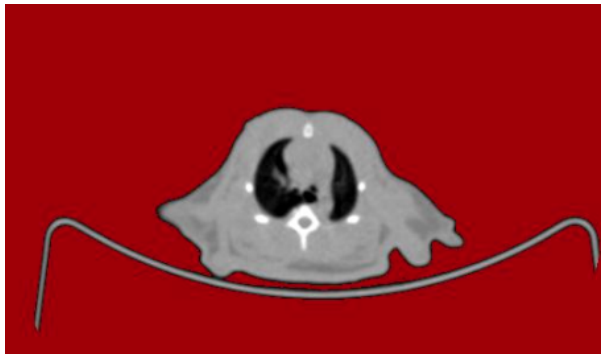

Fig. 5. Results obtained using HU feature only.

representing intensity information. Although grayscale images, in general, have 256 possible intensities values for a pixel, CTs slices are stored in DICOM file which usually has a 12-bit field for the pixel value, so in this case, there are 4096 possible values for each voxel.

The first value in the feature vector is the HU voxel intensity. The next three features in the vector consider statistical information about the voxel being analyzed: the minimum, maximum and mean value computed from its value and the 26 neighbors voxels around it.

The last feature, called depth, represents the position that the voxel sits in the tomography's z-axis. This feature was added later to improve the efficiency of lung segmentation. Because using features based only on HU intensity a dilemma could appear. If the defined threshold value is enough to include the lung edge in the region, then the growth could spread to the upper body through the trachea and nasal pathways. This happened because these areas have intensity values similar to the lung.

With the use of a depth-based feature, it was possible to contain growth only in the lung region. The depth feature also weighs twice as much as the other features when calculating the distance.

Thus, the five features computed from the window of any voxel is a features vector. Then, a new voxel belongs to lung region, if the euclidean distance of its feature vector to the seed's feature vector is less than of a tolerance threshold, as previously described.

This new configuration of the feature vector proved to be more efficient in targeting the target area, as will be presented in the section IV.

B. Parallel Region Growing

Volumetric growth allows greater efficiency in lung segmentation as it helps to avoid the problem where the same organ appears separated in more than one area of the image, which is the case of images with both right and left side of lung in the same image. However, processing growing region segmentation in three dimensions requires a high processing capacity. Since each slice of a CT scan has dimensions of 512 x 512 and in general each scan has about 300 slices, running

this algorithm sequentially can take a long time, because it is necessary to traverse each of the region neighbor voxels at each growth cycle. A 300-slice exam, for example, has 78,643,200 elements, so this is a case in favor of using parallel computing.

Other works such as [18] have already proven the advantage of using parallel processing based on GPUs to accelerate region growing. GPUs are powerful and accessible parallel devices. Their architecture are composed of several thousands cores, grouped in Streaming Multiprocessors (SM). Compute Unified Device Architecture (CUDA) programming model is based on a kernel, that is instantiated in many threads. Each thread is processed by one GPU core. Threads can be grouped, in order to share fast memory data interchange. These groups are called blocks and each block is designated to a specific SM. Each thread is addressed by a thread index. Typical GPU based solutions distribute the data of a large dataset through the thread indices.

In the algorithm proposed in this work, each voxel in the CT Scan volume is mapped to a specific thread index, ensuring that each voxel will be processed in parallel. As the dataset used is a volume, it was used a 3D grid of blocks in CUDA programming language in order to make the code more readable.

In the parallel processing, every voxel of each slice of the scan is processed simultaneously. This factor brings a significant gain in the processing time. Processing occurs at every loop of the region growing algorithm and at each iteration of the loop, all neighboring voxel in the region has the distance from its feature vector to the seed's feature vector calculated. If the distance is less than a predefined threshold, the voxel is included in the region. Algorithm 1 presents the parallel 3D seeded region growing algorithm used in this work.

The *N* is used to define the *scanned* and *region* sizes in the algorithm and corresponds to the number of scan slices, which can vary from exam to exam. The features function used in the algorithm is simply a function that calculates the values in each features vector. The full algorithm implementation can be accessed on this Github repository [19].

Algorithm 1: Parallel 3D Seeded Region Growing Algorithm

Result: The $segmented$ region
input : $scanned$ volume of size $512\times512\times N$
input : Manually selected $seeds$

$region \leftarrow$ new empty volume of size $512\times512\times N$;
for *each seed in seeds* **do**
    $seed\_idx \leftarrow$ *seed*'s index;
    $region[seed\_idx] \leftarrow$ seed number;
end
while *new elements are being included in region* **do**
    `// call CUDA region growing kernel`
    `regionGrowing(`*scanned, region*`)`;
end
return $region$;
Kernel *regionGrowing(scanned, region)* **is**
    $idx \leftarrow$ index based on GPU's thread and block;
    if *element at idx is a region's neighbor* **then**
        $vec1 \leftarrow$ `features(`*scanned, idx*`)`;
        $seed\_idx \leftarrow$ *seed*'s index;
        $vec2 \leftarrow$ `features(`*scanned, seed_idx*`)`;
        $dist \leftarrow$ euclidean distance between $vec1$, $vec2$;
        if $dist < threshold$ **then**
            $region[idx] \leftarrow$ *seed*'s number;
        end
    end
end

IV. Results and Evaluation

To evaluate the efficiency of the proposed method, a set of rodent chest CT scans was used as the evaluation dataset. A ground truth (GT) was created by a manual segmentation procedure, performed on this dataset by a medical specialized in lung images, in order to be used in the evaluation. Ground truth is a set of images where the voxels that represent the correct area to be segmented with the computer program are specified. Finally the parallel 3D seeded region growing method was applied to the CT scans of the five rodents in this dataset.

There are some metrics options in the literature to evaluate the performance of anatomical structure segmentation methods in images, such as the Efficiency (EFI) [20] and Youden indexes. The ROI-index [20] will be used together with Dice similarity coefficient [21] to evaluate the segmentation method proposed in this work. While DICE is the most used metric in validating medical volume segmentation [22], the ROI-Index provides a simpler and more intuitive notion of correctness of the segmentation results [20].

The ROI-Index and DICE coefficient are calculated based on the following basic metrics: true positives (TP), true negatives (TN), false positives (FP) and false negatives (FN). These metrics are based on the classification of each voxel of the scan in which the segmentation was performed. The four basic metrics are explained in more detail in the next paragraphs.

True positives are the voxels that are part of the segmented area both in the ground truth as in the area segmented by the program. Likewise, true negatives are voxels that are not within the area indicated by the program and are also not contained in the ground truth's segmented area.

False positives and false negatives are voxels that are incorrectly classified by the program when compared to the ground truth. False positives are voxels within the area segmented by the program, while false negatives are those outside the area segmented by the program.

The four basic metrics TP, TN, FP, and FN are used to calculate three composite metrics, necessary for the calculation of the ROI-Index, they are Accuracy (ACC) (1), positive predictive (PDP) (2) and negative predictive (PDN) (3).

$$ACC = (TP + TN)/(FN + FP + TN + TP) \quad (1)$$

$$PDP = TP/(TP + FP) \quad (2)$$

$$PDN = TN/(TN + FN) \quad (3)$$

ROI-Index is calculated based on ACC, PDP, and PDN, according to (4). This index was developed focusing on the evaluation the efficiency of a program to segment what it is expected to be in a Region of Interest (ROI) for diagnostic purpose.

$$\text{ROI-Index} = 100 \times (1 - ACC \times PDN \times PDP) \quad (4)$$

DICE similarity coefficient is calculated based on TP, FP and FN according to (5). This index provides a simple and useful measure of spatial overlap, which can be applied to studies of reproducibility and accuracy in image segmentation [23].

$$\text{DICE} = 2 \times TP/(2 \times TP + FP + FN) \quad (5)$$

Five rodent tomographies were used to evaluate the segmentation method proposed in this paper. We made this dataset publicly available in DICOM format in [19].

During the tests, the technique proposed in this paper was used to segment the lung area of five rats. The rodent identified as Animal 01 was selected for a more detailed analysis, based on the ROI-Index, DICE and processing time.

The lung tomography of the individual Animal 01 has 329 slices, with the lungs beginning to appear from slice 122. Starting at slice 122, eight slices were sampled for the performance analysis of the method: 122, 125, 128, 131, 134, 137, 140, 143.

After running the parallel segmentation, the metrics ACC, PDP and PDN were calculated to obtain the ROI-Index for each of the sampled slices. To provide a more comprehensive comparison, DICE coefficient, Efficiency and Youden indexes where also considered in the evaluation. The results are shown in Table I.

TABLE I
RESULTS OF THE ANIMAL 01 SEGMENTATION

#	Efficiency	Youden	ROI-Index	DICE
122	0.814	0.628	24.401	0.687
125	0.896	0.793	0.313	0.884
128	0.892	0.783	0.378	0.879
131	0.873	0.746	3.518	0.844
134	0.892	0.785	0.820	0.878
137	0.904	0.809	0.630	0.894
140	0.912	0.823	0.914	0.902
143	0.936	0.872	0.864	0.930

In general, the similarity indexes showed interesting values. Slice 143, for example, obtained the best similarity between the segmentation performed automatically and the ground truth is very close accordingly both Efficiency, Youden, and DICE coefficient. Fig. 6 shows in green the segmented area using the technique presented in this work and in red the segmented area annotated in the ground truth for slice 143.

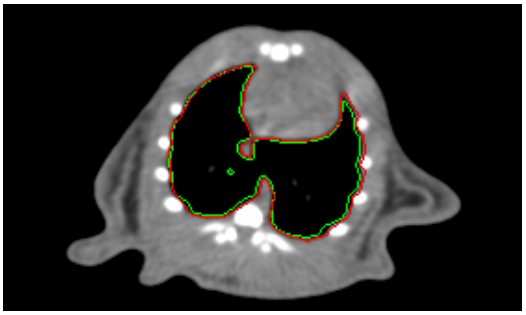

Fig. 6. Animal 01 slice 143, Automatic Segmentation and GT.

Slices 125 and 122, respectively, correspond to the lowest and highest value obtained from the perspective of the ROI-Index, which is why they deserve more attention in the analysis. In regard to the ROI-Index, the lower the value obtained, the greater the similarity between the segmented area and the ground truth.

Fig. 7 shows in green the segmented area using the technique presented in this work and in red the segmented area annotated in the ground truth. It is possible to see in Fig. 7 that the contours are very close to each other.

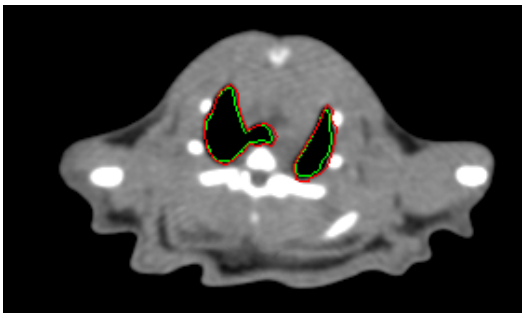

Fig. 7. Animal 01 slice 125, Automatic Segmentation and GT.

Slice 122 showed a relatively high ROI-index compared to other slices. This result was achieved mainly because the area segmented by the program presents some false positives in the tracheal area, as can be seen in Fig. 8.

The trachea region is no longer considered part of the lung, despite having HU values similar to the voxels located within the lung area. To improve the results on this issue, besides tuning the depth feature weight, it may be necessary to consider new ways to stop the growth of the region from a seed in the lung before it leaves the lungs region.

Processing time is an important aspect when applying a segmentation technique. In order to evaluate the performance of the proposed algorithm from the perspective of time, a comparison of processing time with a sequential region growing algorithm, typically used by programs that run on CPUs, was performed.

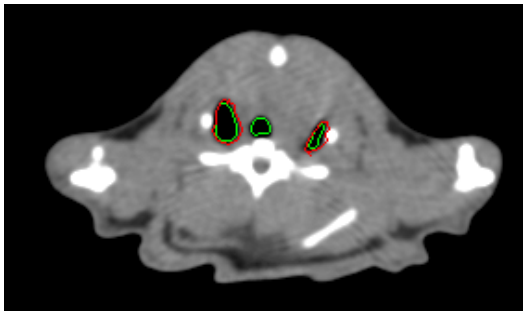

Fig. 8. Animal 01 slice 122, Automatic Segmentation and GT.

The parallel region growing algorithm was implemented using CUDA and then executed on an Nvidia GPU. Results show a considerable performance improvement.

To confirm the performance advantage of using the parallel algorithm over the sequential approach, both techniques were performed on CT scans with 200, 300 and 400 slices. The test results can be seen in the Table II.

TABLE II
PROCESSING TIME COMPARISON

Number of Slices	Sequential	Parallel
100	774.853s	2.588s
200	1457.028s	5.463s
300	1666.775s	11.605s

These tests were performed using the Google Colaboratory [24] cloud environment. The equipment provided by this platform was an Nvidia Tesla P100 GPU, with 6.0 Compute Capability and 16GB RAM.

It is possible to observe the great difference in execution time between the two algorithms, with the parallel approach being at least 150 times faster. The processing time of the sequential algorithm is very high, so the implementation in parallel can be a deciding factor for the adoption of the 3D region growing technique.

V. CONCLUSION

This paper proposes a novel method for the parallel 3D seeded region growing segmentation of anatomical structures, based on GPU architectures. The results observed with a sample of five CT scans of rodents showed that the method is promising both in terms of efficiency in correctly segmenting the region and in the processing time when compared to a sequential algorithm. The improvement of the segmentation technique mainly at the edges and transition areas of the anatomical structure are interesting topics for future work. In near future, we expect to improve our technique using multiple GPUs and more efficient memory access patterns, in order to achieve close to real time processing time.

ACKNOWLEDGMENT

This work is supported in part by CNPq, INCT-MACC, CAPES, FAPERJ and CGI/FAPESP.

REFERENCES

[1] C. Beltran-Perez, H.-L. Wei, and A. Rubio-Solis, "Generalized Multiscale RBF Networks and the DCT for Breast Cancer Detection," *International Journal of Automation and Computing*, vol. 17, no. 1, pp. 55–70, 2020.

[2] C. Botha and B. Preim, *Visual computing for medicine*. Morgan Kaufmann, 2 ed., 2013.

[3] P. S. NEMA, "ISO 12052, Digital Imaging and Communications in Medicine (DICOM) Standard, National Electrical Manufacturers Association (NEMA), Rosslyn, VA, USA," *The operator is provided with a set of worklist items matching the query request*, 2015.

[4] O. Elsayed, K. Mahar, M. Kholief, and H. A. Khater, "Automatic detection of the pulmonary nodules from CT images," in *2015 SAI Intelligent Systems Conference (IntelliSys)*, pp. 742–746, IEEE, 2015.

[5] G. N. Hounsfield, "Computed medical imaging. Nobel lecture, December 8, 1979.," *Journal of computer assisted tomography*, vol. 4, no. 5, p. 665, 1980.

[6] N. Mesanovic, M. Grgic, H. Huseinagic, M. Males, E. Skejić, and S. Muamer, "Automatic CT Image Segmentation of the Lungs with Region Growing Algorithm," in *18th International Conference on Systems, Signals and Image Processing-IWSSIP*, pp. 395–400, 2011.

[7] S. A. El-Regaily, M. A. Salem, M. H. Abdel Aziz, and M. I. Roushdy, "Survey of computer aided detection systems for lung cancer in computed tomography," *Current medical imaging reviews*, vol. 14, no. 1, pp. 3–18, 2018.

[8] S. Farooq and S. Khan Z, "A Survey of Computer Aided Diagnosis (Cad) of Liver in Medical Diagnosis," *VAWKUM Transactions on Computer Sciences*, vol. 15, no. 3, pp. 130–136, 2018.

[9] T. Manikandan and N. Bharathi, "A survey on computer-aided diagnosis systems for lung cancer detection," *International Research Journal of Engineering and Technology*, vol. 3, no. 5, pp. 1562–1570, 2016.

[10] Medixant, "RadiAnt DICOM Viewer."

[11] R. Pradeebha and S. Karpagavalli, "Classification of Lung Disease using Local and Global Descriptors," *International Journal of Computer Applications*, vol. 135, no. 6, pp. 19–23, 2016.

[12] S. Hu, E. A. Hoffman, and J. M. Reinhardt, "Automatic lung segmentation for accurate quantitation of volumetric X-ray CT images," *IEEE transactions on medical imaging*, vol. 20, no. 6, pp. 490–498, 2001.

[13] C. Qin, D. Yao, Y. Shi, and Z. Song, "Computer-aided detection in chest radiography based on artificial intelligence: a survey," *Biomedical engineering online*, vol. 17, no. 1, p. 113, 2018.

[14] A. Conci, E. Azevedo, and F. Leta, *Computer Graphic: Theory and practice*. Ed. Campus Elsevier, Rio de Janeiro, ISBN 978-85-352-2329-3–2008, 2008.

[15] L. Shapiro, "Computer Vision," *New Jersey, Prentice-Hall, ISBN 0-13-030796-3*, 2001.

[16] R. Adams and L. Bischof, "Seeded region growing," *IEEE Transactions on pattern analysis and machine intelligence*, vol. 16, no. 6, pp. 641–647, 1994.

[17] J. R. González, E. O. Rodrigues, and A. Conci, "An algorithm for MRI segmentation based on region growing and anatomical information," *In: 10th International Workshop on Multimedia and Signal processing REDZUR 2016, Bratislava, Slovakia*, 2016.

[18] S. Park, J. Lee, H. Lee, J. Shin, J. Seo, K. H. Lee, Y.-G. Shin, and B. Kim, "Parallelized seeded region growing using CUDA," *Computational and mathematical methods in medicine*, vol. 2014, 2014.

[19] P. Lacerda, "Parallel 3D Region Growing." https://github.com/placerda/region-growing, 2020.

[20] A. Conci, S. S. Galvão, G. O. Sequeiros, D. C. Saade, and T. MacHenry, "A new measure for comparing biomedical regions of interest in segmentation of digital images," in *Discrete applied mathematics*, vol. 197, pp. 103–113, Elsevier, 12 2015.

[21] L. R. Dice, "Measures of the amount of ecologic association between species," *Ecology*, vol. 26, no. 3, pp. 297–302, 1945.

[22] A. Aziz Taha and A. Hanbury, "Metrics for evaluating 3D medical image segmentation: analysis, selection, and tool," 2015.

[23] K. H. Zou, S. K. Warfield, A. Bharatha, C. M. C. Tempany, M. R. Kaus, S. J. Haker, W. M. Wells III, F. A. Jolesz, and R. Kikinis, "Statistical validation of image segmentation quality based on a spatial overlap index1: scientific reports," *Academic radiology*, vol. 11, no. 2, pp. 178–189, 2004.

[24] Google, "Google Colaboratory," 2020.